JACS
JOURNAL OF THE AMERICAN CHEMICAL SOCIETY
Article
Cite This: J. Am. Chem. Soc. 2018, 140, 10497−10503
pubs.acs.org/JACS

In-Cell Titration of Small Solutes Controls Protein Stability and Aggregation

Shahar Sukenik,[†] Mohammed Salam,[†] Yuhan Wang,[‡] and Martin Gruebele*[,†,‡,§]

[†]Department of Chemistry, University of Illinois, Urbana, Illinois 61801, United States
[‡]Center for Biophysics and Quantitative Biology, University of Illinois, Urbana, Illinois 61801, United States
[§]Department of Physics, University of Illinois, Urbana, Illinois 61801, United States

Supporting Information

ABSTRACT: The components of the intracellular environment vary widely in size: from large multiprotein complexes to atomic ions. Besides water, low-molecular-weight solutes (<1 kDa) such as electrolytes, metabolites, and carbohydrates are by far the most abundant of these components. Small solutes are thus key contributors to the solvation environment in the cell. Small solutes have been known for decades to alter protein structure or activity *in vitro*, through their interactions with protein surfaces or hydration shells. Here we use the cell itself as our test tube, by titrating its hydration, ion, or carbohydrate composition systematically. We trigger the selective uptake of specific solutes by exposing cells to hyperosmotic media. We then measure protein structure, stability, unfolding kinetics, and aggregation in these different intracellular environments by using fast relaxation imaging. We compare these results with controls where solutes cannot enter the cell and only hydration is altered. Protein structure, thermal stability, and aggregation onset all depend on the concentration and chemical nature of the solute titrated into the cell. Our work highlights the important contributions of small solutes in defining how proteins interact within the cell and suggests that intracellular variation of the solute composition could be an important regulator of protein function.

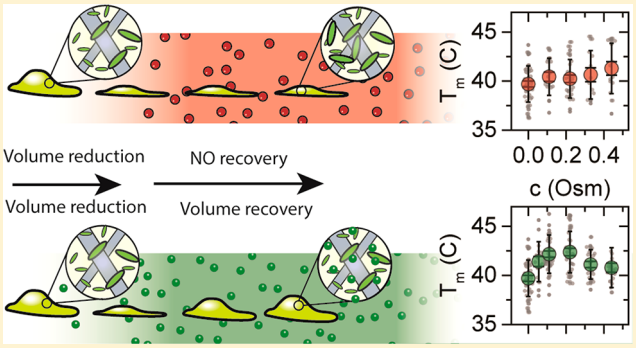

Proteins, the macromolecules that enable life, interact with solvation water and with small solutes (MW < 1 kDa) such as ions, metabolites, nucleotides, amino acids, and other naturally occurring organic molecules.[1,2] Well-documented examples of effects in buffered solutions include salting out,[3] denaturant-induced unfolding (e.g., urea[4,5] or dodine[6]), and osmolyte-induced stabilization.[7−9] Simulations[5,10] and single-molecule[11] and ensemble-averaged experiments[12,13] all highlight a spectrum of structural and activity changes that occur as a result of changes to small solute composition. In the cell, small solutes dominate the solvation environment, by virtue of their fast diffusion[14] and large numbers (>10 mM for a single solute is not uncommon,[15] compared to <10 mM for the entire protein population in a cell[16]). The small solute population is in constant flux, due to both internal (e.g., cell cycle[17]) and external factors (e.g., environmental stress response of membrane channels[18]). Although the free energy changes to protein structure due to solute composition changes are expected to be subtle (∼10 kJ/mol per mole of solute), the energy landscapes of proteins often have small barriers and shallow minima and can thus be modulated significantly by solvation conditions.[19,20]

Highlighting the importance of the cellular environment for protein activity, recent studies point to a measurable effect of abundant solutes on proteins in the cell.[21−25] The *in vitro* approach to elucidate how small solutes alter protein dynamics involves titrating a single solute into a test tube, while keeping other factors in the experiment fixed; controlling the cellular milieu in an equally reproducible and quantifiable way is a challenging task, although it has been shown to be possible in certain cases.[24,26−28]

Here we perform in-cell titration of a single solute by exposing cells to hyperosmotic media of different compositions. We supplement cell media with different concentrations of the carbohydrates/polyols galactose (gal) or mannitol (man) or the salts KCl or NaCl. Live cell microscopy shows that while man and NaCl are excluded from the cell, gal and KCl are taken up over the course of ∼15 min, up to the point of complete cell volume recovery. Once volume has recovered, the total osmotic pressure in the cell is equal to that in the surrounding media, allowing us to estimate the in-cell concentration of the uptaken solute K^+ or gal. By tuning the media's hyperosmolarity, we can titrate permeable solutes into the cell's interior. Impermeable solutes such as Na^+ and man in contrast dehydrate the cell interior by volume reduction.

To see if solute uptake modulates protein structure and stability, we use fast relaxation imaging (FReI)[29] in cells

Received: May 12, 2018
Published: July 25, 2018

DOI: 10.1021/jacs.8b04809
J. Am. Chem. Soc. 2018, 140, 10497−10503

transiently expressing fluorescence resonance energy transfer (FRET)-labeled phosphoglycerate kinase[30] (fPGK). PGK is a ubiquitous glycolytic enzyme that can catalyze both its forward and reverse reactions dependent on ATP/ADP ratios.[31] The cells are incubated in different hyperosmotic media and subjected to rapid temperature jumps while collecting the FRET signal from in-cell fPGK. Analysis of fPGK FRET curves from live cells shows that cells incubated in hyperosmotic, cell-excluded solutes man and NaCl behave very similarly in response to temperature change, despite the disparate chemical nature of these solutes. This contrasts with the solutes' behavior *in vitro*, when they are in direct contact with the protein. Thus, the effect of such controls on fPGK in the cell stems from mainly the changes induced to the cell by hyperosmotic pressure (e.g., increased crowding). In contrast, the uptaken solute gal shows behavior different from the uptaken solute KCl, and their effect is in some cases similar, in others different, from their effect *in vitro*. We can thus control the in-cell concentration of certain solutes and monitor their effect on protein stability and kinetics.

METHODS

Protein Expression and Purification. BL21 (DE3)-RIPL cells (Agilent) were transfected according to manufacturer-supplied protocols with pDream2.1 plasmids (Genscript). The plasmid confers ampicillin resistance and contained either fPGK or fCrH2 genes (sequences described previously[21]) inserted between NotI and *Bam*HI restriction sites. All expressed proteins contained a 6x-His tag and a thrombin cleavage site at the N-terminus. Cells were grown at 37 °C to OD 0.6 in selective LB media, then induced using IPTG and incubated at 16 °C overnight. The cells were then lysed using a tip sonicator and spun down, and the filtered lysate was purified using an AKTA FPLC with a His-trap affinity chromatography column (GE Healthcare). Purified proteins were dialyzed into 3 × 4 L of phosphate-buffered saline (PBS) buffer. The identity of the purified protein was verified using SDS-PAGE and MALDI-TOF mass spectrometry.

Materials. Mannitol was purchased from Sigma, galactose was from Acros, and KCl and NaCl were from VWR and used without further purification. Dulbecco's modified Eagle's medium (DMEM) was purchased from Corning and supplemented with penicillin streptomycin antibiotics (5%), pyruvate (1 mM), and fetal bovine serum (10%).

Fluorimetry. All *in vitro* fluorescence was measured using a Jasco FP-8300 fluorimeter equipped with a four-cell holder with Peltier temperature control. In all cases, the sample was excited by 450 nm light, and emission was scanned between 480 and 700 nm. In both excitation and emission the slit width was 5 nm. Temperature scans were performed between 20 and 65 °C in steps of 3 °C, with a 5 min wait prior to each scan to ensure temperature equilibration. FRET signal was obtained by fitting the raw fluorescence signal to two gaussians centered at 515 and 600 nm. The peak heights were detected, and the ratio between the heights was taken as the *in vitro* D/A ratio. This value differed from that found on the microscope due to light source intensity, detector sensitivity, and imaging path differences, but the trends remained similar. To verify the analysis method, D/A ratio was also obtained by taking the integrated fluorescence emission at <580 nm as D and at ≥580 nm as A. This analysis showed little or no change compared with the one obtained by maximal peak value.

Cell Line Handling and Transfection. U-2 OS cells (ATCC) were grown and passaged in DMEM supplemented with 10% fetal bovine serum (Sigma) and 5% penicillin/streptomycin (P/S, Sigma). Cell lines were passaged every 3 days and used for up to 30 passages before discarding.

Live Cell FReI Experiments. Cells were transfected in 75 cm^2 flasks 17−26 h prior to imaging with the appropriate plasmid using standard Lipofectamine 2000 protocol (Thermo-Fisher). After 5−6 h of incubation, cells were trypsinized and replated on precleaned 25 × 25 mm #1.5 coverslips. Prior to imaging, coverslips containing fCrH2 or fPGK-expressing cells were washed twice with PBS, then with either neat Fluorobrite media (FB, Gibco) or FB supplemented with appropriate osmotic agents and sealed face down on a slide using 120 μm thick double-sided spacer stickers (Grace Biolabs). Cells were immediately imaged (for fCrH2 measurements) or allowed to recover their volume for 15 min following exposure and then placed on the FReI microscopy setup described previously.[32,33] Briefly, FReI is based on an inverted epifluorescent microscope (Zeiss Axiovert 100 TV), with a 2200 nm IR diode laser (Thorlabs) mounted from the top and focused onto the sample. Upon triggering, the laser amplitude is modulated to achieve sharp increases in temperature to obtain step-like behavior. Fluorescence is collected by exciting cells at 470 nm using a blue LED (Thorlabs), and emission is split downstream using a 550 nm dichroic (Chroma), then directed into two adjacent spots on a Phantom V12.1 CMOS camera. Experiments are performed at 60 fps using a 63× N-Achroplan air-immersion objective, NA 0.85 (Zeiss).

Image Analysis. Details are described in Figure S1. The full data set, including raw data, analyses, and all analysis scripts for FReI experiments in MATLAB format, is available online at http://doi.org/10.13012/B2IDB-4308433_V1. The cell-by-cell temperature calibration procedure for FReI experiments is described in Figure S2.

Live Cell Volume Recovery Experiments. To prevent an osmotic pressure gradient during imaging, as may be caused by uneven concentrations when pipetting hyperosmotic media into the cell, we use a computer-controlled flow cell to image cellular volume changes in real time. U-2 OS cells were plated onto μ-slide$^{0.2}$ I (ibidi) flow cells to a final confluency of ∼30−40%, allowed to adhere overnight, then labeled using Calcein AM and/or DiI dyes (Molecular Probes, Inc.) according to manufacturer's protocol. Cells were then allowed to recover in serum-supplemented DMEM and imaged up to 2 h after dye loading. Live cell 3D imaging of volume recovery was done on a Zeiss LSM 880 equipped with an Airyscan detector running in fast acquisition mode. Imaging was done in one or two channels (depending on the dyes used), using a 488 and 560 nm laser line, and a 40× N-Achroplan 1.4 NA water immersion objective. Isosmotic FB media was allowed to flow by gravity for ∼2 min. The flow was stopped, and the reservoir was filled with the hyperosmotic media. About 5 mL of the hyperosmotic media was allowed to flow through the flow cell during imaging, and the flow stopped again. The total volume of the tubing and the flow cell is less than 1 mL, and so at this point the cells are immersed in hyperosmotic media. The cells were then imaged for an additional 20−60 min. To obtain 3D images, stacks at 1−2 Airy units, ∼15 μm in height, were collected every 30 s.

Data Fitting. All melting curves were fit using a sigmoidal curve with sloping baselines using either OriginPro or Matlab. For the in-cell melting curves shown in the main text, the sigmoidal contained a sloping baseline for the folded ensemble, and a fixed baseline was set at the maximal D/A value for the unfolded ensemble to diminish the effects of aggregation (see Discussion). All kinetic traces were fit at their maximal amplitude to a double-exponential decay.

RESULTS

Certain Solutes Are Internalized by the Cell within Minutes of Hyperosmotic Exposure. To characterize the uptake of specific solutes into cells in real time, we rely on the rapid uptake of solutes that can enter the cell through either membrane permeability or specific channels in the cell's membrane.[18,24,34] Uptake is rapid only for specific ions and small organic molecules (such as cyclic sugars and other molecules known to internalize into the cell), allowing us to tailor the experiments into three groups: crowding-only controls, when the solute is not taken up; cell-as-a-test tube measurements, when the solute is taken up, increasing that

DOI: 10.1021/jacs.8b04809
J. Am. Chem. Soc. 2018, 140, 10497−10503

solute's concentration in the cell; and the iso-osmotic control before cell volume and solute content have been altered.

To induce the increased uptake of solutes into the cell, we incubate U-2 OS cells in hyperosmotic solutions. Following volume reduction due to hyperosmotic exposure, cells will uptake permeable solutes up to the point at which the internal osmolarity of the cell is equated to the external osmolarity. On the other hand, impermeable solutes will result in long-term reduced cell volume after water is expelled to reduce osmotic pressure. To verify that this uptake occurs as predicted, we image cells during the onset and subsequent recovery from exposure to various hyperosmotic media using fast 3D confocal microscopy (see Methods). Figure 1a shows volume decrease

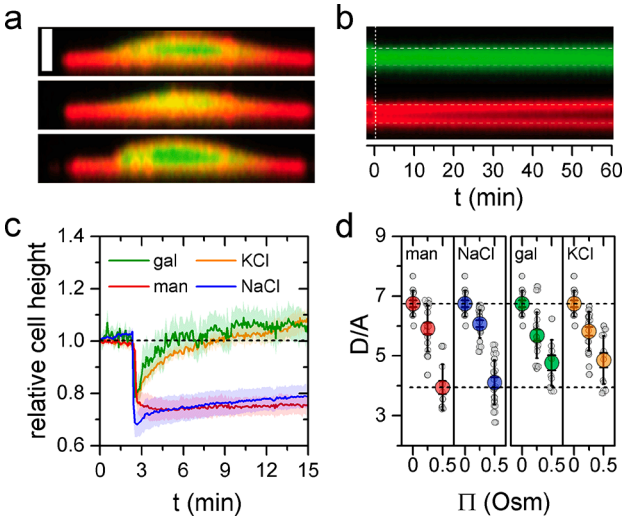

Figure 1. Volume recovery of U-2 OS cells exposed to hyperosmotic media. (a) Cross sections of a calcein (green)- and DiI (red)-labeled cell before, immediately following, and 1 h after exposure to DMEM with 220 mOsm KCl (see Methods for details). Scale bar is 10 μm. (b) Kymograph of the same cell showing volume recovery in the cytoplasm (top) and height changes in the membrane (bottom); the vertical dashed line at t=0 represents the onset of hyperosmotic stress; the horizontal dashed line is aligned with initial cell height (c) Cell height time traces for different hyperosmotic media (Figure S3), normalized to height at isosmotic conditions. Lines are averages; shaded area is the SD of at least three cells; the horizontal dashed line indicates initial cell height. (d) Live cell fCrH2 FRET signal at ≥15 min. Data from individual cells are shown in gray. In all box charts in this paper, averages are denoted by colored circles, and short and long whiskers represent SD and SE of the data, respectively. Dashed line denotes the minimal and maximal average D/A values for the data set.

and recovery of a slice across a U-2 OS cell upon exposure to a hyperosmotic pressure of 200 mOsm KCl. With this solute, volume recovery is rapid over the course of ~15 min, as shown in the kymograph in Figure 1b. Once the volume has recovered, the cell returns to steady state for the next ~45 min in which we perform our experiments. At longer incubation times, cells can show loss of adhesion, blebbing, and loss of calcein fluorescence, indicating depletion of ATP and cell death.

To quantify the rate and extent of volume recovery, cross sections were obtained from cells incubated with a variety of hyperosmotic media, and the cell height from 10 points along these cross sections was tracked and averaged over time (see Figure S3). Cell height traces, shown previously to be a good proxy of cellular volume change[35] (Figure S4), are shown in Figure 1c. These traces show that both KCl and gal, a cyclic sugar known to be rapidly internalized as an energy source in the cell,[34,36] show a rapid volume recovery over the course of ~15 min. NaCl showed little or no volume recovery, implicating the K^+ ions in the volume recovery observed for KCl. Man, a linear sugar alcohol commonly used to diminish swelling in brain tissue due to its ability to induce hyperosmotic pressure,[37] also showed little or no recovery during the course of the experiment.

We used the crowding sensor fCrH2[21,38] to measure the crowding conditions in cells at the onset of hyperosmotic pressure (Figure 1d). fCrH2 contains two fluorescent proteins that form a FRET pair on its N- and C-termini. With FRET, a lower donor (green) to acceptor (red) ratio (D/A) ratio corresponds to a shorter distance between the terminal AcGFP and mCherry tags. Upon increased crowding (reduced free volume),[39] fCrH2 is designed to contract, bringing the donor and acceptor closer on average and decreasing D/A. For both KCl and gal, the intracellular environment is significantly less crowded at the highest osmotic stress tested (P = 0.02) than for man and NaCl, as shown by D/A of fCrH2 (Figure 1d). In the man/NaCl case, the solutes are not taken up and crowding increases, whereas in the gal/KCl case solutes and water are taken up after a short delay, and the crowding increases less.

fPGK *in Vitro* Displays Distinct Thermal Stability Curves in Carbohydrates vs Salts. To understand how changes to intracellular solution composition affect proteins in the cell, we look at the D/A of FRET-labeled PGK, a ubiquitous glycolytic enzyme.[30] We label PGK with AcGFP1 and mCherry on its C- and N-termini. The FRET signal of the labeled construct (fPGK) reports on structural changes, including unfolding, and is also correlated with its enzymatic activity.[29]

We begin by assessing the effect of the four classes of solutes on fPGK structure and stability in a buffered aqueous solution: KCl (salt, cell-penetrating); NaCl (salt, nonpenetrating); gal (carbohydrate, cell-penetrating); man (carbohydrate, non-penetrating). We recombinantly expressed and purified fPGK in PBS solutions with increasing concentrations of the different solutes used in our live cell experiments (Methods). For each concentration, a melting curve was measured via the ratio of donor to acceptor fluorescence, Figure 2a. The curves were fit to sigmoidal functions, as described in Methods.

The folded (F, <30 °C) and unfolded (U, >45 °C) baseline values for D/A, which monitor structural changes as a function of solute concentration, show little or no change for all solutes tested (Figure 2b,c). This indicates that outside the cell the addition of either salt or polyol does not significantly change the folded or the unfolded structure of the protein. The melting temperature (T_m) showed distinct behaviors based on chemical similarity, Figure 2d. Both salts caused little change in T_m, while the carbohydrates man and gal caused a linear, concentration-dependent increase, a stabilizing effect similar to that observed for osmolytes.[9,19]

fPGK Stability and Structure Are Affected by the Intracellular Environment. As seen in Figure 2b, none of the four solutes have much effect on fPGK folded structure, and only the two carbohydrates affected T_m. Thus, we hypothesized analogous behavior in-cell for the two cell-penetrating solutes: gal would have a stabilizing effect, but KCl would not cause this change except at very high osmolarity, where crowding becomes significant (Figure 1d). Man and

DOI: 10.1021/jacs.8b04809
J. Am. Chem. Soc. 2018, 140, 10497−10503

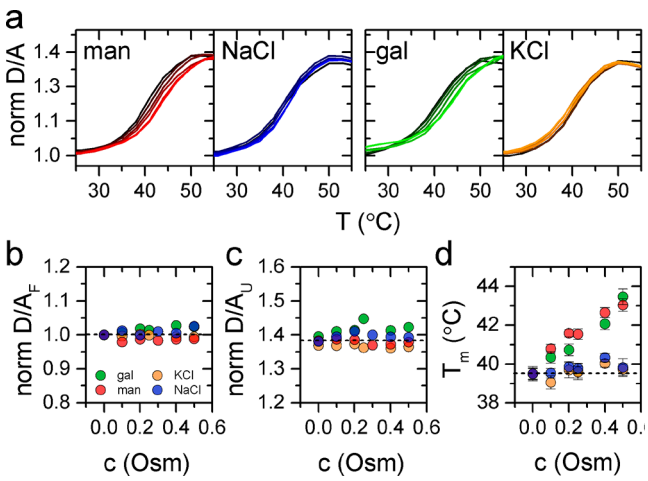

Figure 2. fPGK melting *in vitro*. (a) D/A of fPGK normalized to its value at the 25 °C signal as a function of temperature in PBS supplemented by different solutes. Curves are 0, 110, 220, 330, and 440 Osm going from dark to bright. (b, c) Normalized D/A in the folded (b) and unfolded (c) ensembles for different solute compositions. (d) fPGK melting temperature, T_m. Error bars are the SD of three repeats. In all bottom panels, colors are the same as panel (a).

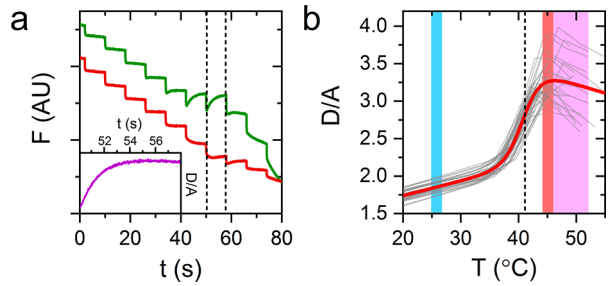

Figure 3. Fast relaxation imaging. (a) Green and red lines are the donor and acceptor fluorescence, respectively. Steps are the response of GFP or mCherry fluorescence to IR laser-induced T-jumps (see Figure S2). Inset shows the D/A following the T-jump between the dashed lines. (b) FRET signal from live cells. The red line is a fit of the entire data set to a sigmoidal with folded and unfolded baselines (see Methods). The blue and red regions indicate the D/A at 25 °C and at maximum value. The dashed line indicates T_m. The pink region indicates the onset of aggregation.

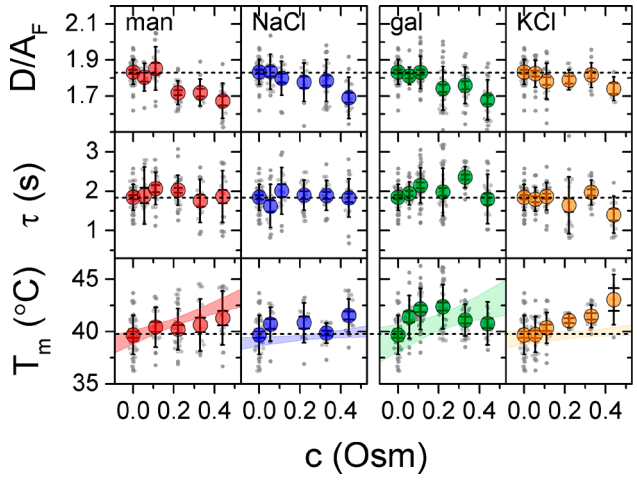

Figure 4. In-cell thermodynamics and kinetics of fPGK in different hyperosmotic environments. (Top) FRET signal of the folded state taken at 25 °C. (Middle) Observed relaxation kinetics at transition maximum (dashed line in Figure 2d). (Bottom) In-cell melting temperature. Shaded region corresponds to the SD of the melting point measured *in vitro* (Figure 2b). Box charts are as those shown in Figure 1d.

NaCl would result in a slight compaction of the native state and increased fPGK stability due to crowding.

To test this hypothesis, we rapidly T-jumped cells expressing fPGK after incubating them for 15−50 min in either hyperosmotic or iso-osmotic media. Figure 3 shows the result for iso-osmotic media. Ten to 12 rapid laser-induced temperature steps mapped out fPGK unfolding (Figures 3a and S2). Cells showed good viability within this time range, as indicated by imaging and a propidium iodide viability assay (Figure S5).

All cells displayed a sigmoidal fPGK unfolding curve (Figure 3b), similar to that observed *in vitro* (Figure 2a). The folded baseline (<35 °C in Figure 3b) slopes slightly upward in the D/A ratio. That observation can be explained quantitatively by the different temperature-dependent quantum yields of AcGFP1 vs mCherry.[40] In contrast, the unfolded state displays a negative slope, which we attribute to unfolded protein aggregation (Figure 3a; see discussion below). Each cell was measured only once due to irreversibility of fPGK melting in the cell under the present conditions,[29] and cells were measured on the same coverslip for up to 50 min following a hyperosmotic challenge. The total data set encompassed in this work comprises ∼400 live-cell fPGK melting experiments in different media.

We first look at the effect of different intracellular environments on the folded structure of fPGK. Unlike Figure 2b, Figure 4 top shows that D/A_F decreases slightly (FRET efficiency increases slightly) in all hyperosmotic solutions. This observation is in line with what was previously reported for fPGK in the presence of synthetic, nonionic crowder Ficoll.[30] For man and NaCl, the decrease of D/A_F can be due only to increased crowding. For gal and KCl, where there is uptake and less crowding (Figure 1b,c), the effect is likely due to a gradual change in intracellular solvation environment, and gal shows a slightly larger effect than KCl. Unlike the folded state, the unfolded state does not show obvious trends (Figure S6). This may be due to the increased noise associated with fPGK aggregation at high temperature (Figure 3b, pink area).

We also measured protein relaxation kinetics (see the inset of Figure 3a) around the unfolding transition (τ, Figure 4 center row) in cells incubated in different hyperosmotic media. We found no dependence of these relaxation rates on increased crowding when man or NaCl was used or on the uptake of gal and KCl. This indicates that neither crowding nor uptake of solutes to the cellular environment significantly alters the rate of protein folding. From the error in the measurements, we can put an upper limit of a factor of ∼1.5 change in relaxation time due to crowding or in-cell solute titration, in all conditions tested. This is in line with changes less than a factor of 2 reported between *in vitro* and in cell experiments on different fluorescent variants of PGK.[41]

The strongest effect of the cellular environment was seen in the melting temperature T_m of fPGK (dashed line in Figure 3b), shown in Figure 4 bottom. Importantly, all T_m values were calculated from both thermodynamics (reported here) and kinetic analysis[42] and show good agreement as detailed in Figure S7. The chemically disparate man and NaCl show very

DOI: 10.1021/jacs.8b04809
J. Am. Chem. Soc. 2018, 140, 10497−10503

similar trends, at most a small increase of T_m, even though their *in vitro* trends were very different (Figure 2d). We attribute this minor change to increased crowding upon cellular volume reduction when solutes are not taken up into the cell. In contrast, cell-penetrating KCl causes T_m to gradually increase, unlike the *in vitro* result. Thus, it is likely that K^+ or Cl^- do not interact differently with fPGK in-cell than *in vitro*, but instead the ions affect the intracellular matrix, which in turn interacts with fPGK. Gal caused a rapid initial increase of fPGK stability (faster even than *in vitro*) followed by a turnover and decline (unlike the *in vitro* result). We rationalize the nonmonotonic T_m with gal in the discussion.

DISCUSSION

The slight stabilization of fPGK when cell volume is simply reduced by using man or NaCl can be explained by the increased crowding in Figure 1d (left two panels). The disparate trend for gal and KCl in both T_m and in the D/A value requires the examination of more complex interactions taking place within the cell.

As one possible contribution to the turnover of T_m with increasing gal concentrations (see Figure 4), we show the ATP/ADP dependence of T_m in Figure 5. PGK (and fPGK[29])

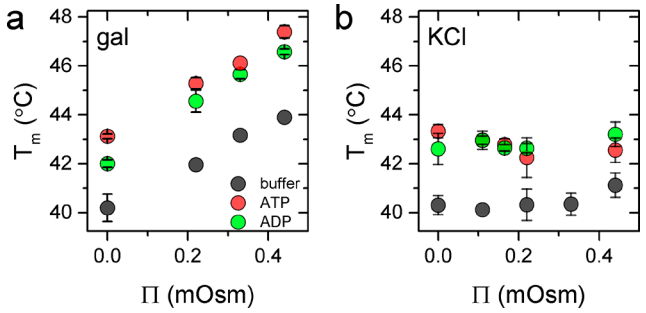

Figure 5. Melting temperature of fPGK in PBS and increasing gal (a) or KCl (b) results with 2 mM ATP (green), 2 mM ADP (red), or neither (black) are shown.

binds ADP during the catalytic cycle. The reaction can also be driven backward by ATP binding.[31] Figure 5 shows that both ADP and ATP stabilize fPGK as the in-cell gal concentration increases, but ATP more so than ADP. Thus, an increase in ADP/ATP concentration ratio, which happens when the cell is under hyperosmotic duress,[43] can act to decrease the melting temperature in the presence of gal (Figure 5a). While the ATP to ADP difference of 1 to 2 °C in Figure 5a is by no means sufficient to account for the full turnover observed in Figure 4, it points to the possibility of interactions with other small solutes to alter protein thermal stability in the cell. In contrast, ATP and ADP show no differential effect when the in-cell KCl concentration increases, and T_m does not turn over when K^+ enters the cell in Figure 4. Thus, KCl stabilizes fPGK irrespective of ATP/ADP ratio. Since no stabilizing effect was observed *in vitro*, K^+ likely acts on the protein indirectly by modifying the properties of the cytoplasmic matrix.

Intracellular aggregation of fPGK is also solute-dependent. When the fPGK population in the cell unfolds, the red fluorescence increases in Figure 3a (<50 °C). The onset of aggregation is seen as an upturn in red and a sharp decrease in green fluorescence as shown in Figure 3a (>50 °C), resulting in a drop in D/A. Upon cooling and subsequent reheating, the initial baseline is not recovered, and transition is no longer observed, as shown in Figure S8. To quantify how intracellular composition alters fPGK aggregation, we measure the slope of the points following the D/A maximum (Figure 3b, pink region) as a proxy for aggregation. Figure 6 shows these slopes

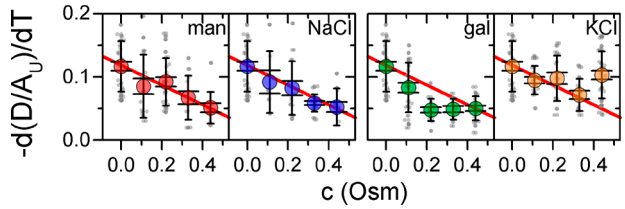

Figure 6. fPGK aggregation. The slope of the unfolded baseline (Figure 3b, pink region) is taken as a proxy to estimate aggregation. Red lines are a linear fit of man slopes.

for different solute compositions. We see a similar effect for NaCl and man (excluded solutes): the propensity of fPGK to aggregate gradually decreases as cell volume decreases and crowding increases. This is counterintuitive: aggregation is a bimolecular or higher order reaction and thus should be driven by reduced volume.[44,45] However, at the same time diffusion is reduced and sticking interactions of fPGK with the cytoplasmic matrix increase, and this may reduce fPGK self-aggregation.

Gal and KCl show different trends. KCl continues to promote aggregation even at high intracellular composition. This is consistent with the lack of increased crowding (compared to man/NaCl). Increased aggregation of proteins in cells in the presence of salts has been recently reported in other experiments.[46,47] In these cases, the presence of ions was thought to mask charge−charge repulsion that can inhibit aggregation (the fluorescent protein labels add significant negative charge to the +1 charge of PGK). It is important to note that this need not contradict the enhanced stability shown for fPGK in the presence of high KCl concentrations. For example, it is possible that the folded state in the presence of KCl is stabilized, yet the unfolded state, once formed, is more prone to aggregation due to reduced screening at higher K^+ concentrations. In contrast, even low concentrations of gal result in a rapid reduction of aggregation. This could be due to the stabilizing effect of gal on the monomeric protein seen at low osmolarity (Figure 4); indeed, carbohydrates such as sorbitol and inositol, which are molecularly similar to galactose, have been previously shown to inhibit and in some case even reverse protein aggregation.[48−50] At high osmolarity, the aggregation propensity ceases to decrease, just as protein stability in Figure 4 turns around.

Another possible contribution to protein aggregate concentration in the cell is that the activity of molecular chaperones depends on solute conditions in the cell, as recently shown for GroEL.[51] Further studies involving metabolomic profiling[15] together with thermal stability[52] measurements will be helpful in resolving these effects.

CONCLUSIONS

Using experiments to monitor protein structure and stability in cells subjected to either a volume decrease (NaCl, man) or increased concentration of specific solutes (KCl, gal), we show that the uptake of small solutes into the intracellular space can alter protein stability in a concentration-dependent manner. Although the effects are small, they can significantly shift equilibria within the cell due to the exponential dependence of

DOI: 10.1021/jacs.8b04809
J. Am. Chem. Soc. 2018, 140, 10497−10503

equilibrium constants on the free energy. Solute balance in cells is thus a potentially important contributor to protein regulation and homeostasis in the cell. Since the effect of many small solutes on protein structure has been well studied *in vitro*, extending these observations to live cells can provide new insight into the way such solutes alter protein stability and folding. Titrating small molecules into cells could help elucidate their effect on other reactions in cells, such as enzymatic catalysis or drug−protein binding interactions. Finally, cell-type-dependent selective uptake of solutes (e.g., that found in kidney[8] or some cancer cells[53]) may even enable targeting of malignancies by disrupting essential protein functions or proteostasis.

All FReI data are available online at http://doi.org/10.13012/B2IDB-4308433_V1.

■ ASSOCIATED CONTENT

Supporting Information

The Supporting Information is available free of charge on the ACS Publications website at DOI: 10.1021/jacs.8b04809.

Image analysis methods and supplemental tables and figures (PDF)

■ AUTHOR INFORMATION

Corresponding Author

*mgruebel@illinois.edu

ORCID

Shahar Sukenik: 0000-0003-3855-9574

Martin Gruebele: 0000-0001-9291-8123

Notes

The authors declare no competing financial interest.

■ ACKNOWLEDGMENTS

The authors thank A. De Vries for use of his osmometer and N. Dolev for help with statistical analysis. We acknowledge A. Cyphersmith and S. Mayandi from Core Facilities at the Carl R. Woese Institute for Genomic Biology for help with live cell volume recovery imaging. This work was funded by the National Science Foundation, grants NSF MCB 1413256 and MCB 1803786.

■ REFERENCES

(1) Davis-Searles, P. R.; Saunders, A. J.; Erie, D. A.; Winzor, D. J.; Pielak, G. J. *Annu. Rev. Biophys. Biomol. Struct.* **2001**, *30*, 271−306.

(2) Timasheff, S. N. *Proc. Natl. Acad. Sci. U. S. A.* **2002**, *99*, 9721−9726.

(3) Nandi, P. K.; Robinson, D. R. *J. Am. Chem. Soc.* **1972**, *94*, 1299−1308.

(4) Tanford, C. *Adv. Protein Chem.* **1968**, *23*, 121−282.

(5) O'Brien, E. P.; Ziv, G.; Haran, G.; Brooks, B. R.; Thirumalai, D. *Proc. Natl. Acad. Sci. U. S. A.* **2008**, *105*, 13403−13408.

(6) Guin, D.; Sye, K.; Dave, K.; Gruebele, M. *Protein Sci.* **2016**, *25*, 1061−1068.

(7) Yancey, P. H. *Integr. Comp. Biol.* **2001**, *41*, 699−709.

(8) Garcia-Perez, A.; Burg, M. B. *Physiol. Rev.* **1991**, *71*, 1081−1115.

(9) Harries, D.; Rösgen, J. *Methods Cell Biol.* **2008**, *84*, 679−735.

(10) Politi, R.; Harries, D. *Chem. Commun.* **2010**, *46*, 6449−6451.

(11) Ferreon, A. C. M.; Moosa, M. M.; Gambin, Y.; Deniz, A. A. *Proc. Natl. Acad. Sci. U. S. A.* **2012**, *109*, 17826−17831.

(12) Sarkar, M.; Lu, J.; Pielak, G. J. *Biochemistry* **2014**, *53*, 1601−1606.

(13) Guinn, E. J.; Pegram, L. M.; Capp, M. W.; Pollock, M. N.; Record, M. T., Jr *Proc. Natl. Acad. Sci. U. S. A.* **2011**, *108*, 16932−16937.

(14) Verkman, A. S. *Trends Biochem. Sci.* **2002**, *27*, 27−33.

(15) Bennett, B. D.; Kimball, E. H.; Gao, M.; Osterhout, R.; Van Dien, S. J.; Rabinowitz, J. D. *Nat. Chem. Biol.* **2009**, *5*, 593−599.

(16) Beck, M.; Schmidt, A.; Malmstroem, J.; Claassen, M.; Ori, A.; Szymborska, A.; Herzog, F.; Rinner, O.; Ellenberg, J.; Aebersold, R. *Mol. Syst. Biol.* **2011**, *7*, 1−8.

(17) Eckel-Mahan, K. L.; Patel, V. R.; Mohney, R. P.; Vignola, K. S.; Baldi, P.; Sassone-Corsi, P. *Proc. Natl. Acad. Sci. U. S. A.* **2012**, *109*, 5541−5546.

(18) Burg, M. B.; Ferraris, J. D.; Dmitrieva, N. I. *Physiol. Rev.* **2007**, *87*, 1441−1474.

(19) Gruebele, M.; Dave, K.; Sukenik, S. *Annu. Rev. Biophys.* **2016**, *45*, 233−251.

(20) Holehouse, A. S.; Pappu, R. V. *Annu. Rev. Biophys.* **2018**, *47*, 1−21.

(21) Sukenik, S.; Ren, P.; Gruebele, M. *Proc. Natl. Acad. Sci. U. S. A.* **2017**, *114*, 6776−6781.

(22) Monteith, W. B.; Cohen, R. D.; Smith, A. E.; Guzman-Cisneros, E.; Pielak, G. J. *Proc. Natl. Acad. Sci. U. S. A.* **2015**, *112*, 1739−1742.

(23) Mu, X.; Choi, S.; Lang, L.; Mowray, D.; Dokholyan, N. V.; Danielsson, J.; Oliveberg, M. *Proc. Natl. Acad. Sci. U. S. A.* **2017**, *114*, E4556−E4563.

(24) Gnutt, D.; Brylski, O.; Edengeiser, E.; Havenith, M.; Ebbinghaus, S. *Mol. BioSyst.* **2017**, *13*, 2218−2221.

(25) Patel, A.; Malinovska, L.; Saha, S.; Wang, J.; Alberti, S.; Krishnan, Y.; Hyman, A. A. *Science* **2017**, *356*, 753−756.

(26) Ignatova, Z.; Gierasch, L. M. *Proc. Natl. Acad. Sci. U. S. A.* **2006**, *103*, 13357−13361.

(27) Stadmiller, S. S.; Gorensek-Benitez, A. H.; Guseman, A. J.; Pielak, G. J. *J. Mol. Biol.* **2017**, *429*, 1155−1161.

(28) Bandyopadhyay, A.; Saxena, K.; Kasturia, N.; Dalal, V.; Bhatt, N.; Rajkumar, A.; Maity, S.; Sengupta, S.; Chakraborty, K. *Nat. Chem. Biol.* **2012**, *8*, 238−245.

(29) Ebbinghaus, S.; Dhar, A.; McDonald, J. D.; Gruebele, M. *Nat. Methods* **2010**, *7*, 319−323.

(30) Dhar, A.; Samiotakis, A.; Ebbinghaus, S.; Nienhaus, L.; Homouz, D.; Gruebele, M.; Cheung, M. S. *Proc. Natl. Acad. Sci. U. S. A.* **2010**, *107*, 17586−17591.

(31) Bücher, T. In *Methods in Enzymology*; Elsevier, 1955; Vol. *415*, pp 415−422.

(32) Ebbinghaus, S.; Gruebele, M. *J. Phys. Chem. Lett.* **2011**, *2*, 314−319.

(33) Dhar, A.; Gruebele, M. *Curr. Protoc. Protein Sci.* **2011**, Chapter 28, Unit 28.1, *65*, 1.

(34) Barros, L. F. *Pfluegers Arch.* **1999**, *437*, 763−770.

(35) Sukenik, S.; Ren, P.; Gruebele, M. *Proc. Natl. Acad. Sci. U. S. A.* **2017**, *m*, 201700818.

(36) Hoffmann, E. K.; Lambert, I. H.; Pedersen, S. F. *Physiol. Rev.* **2009**, *89*, 193−277.

(37) Francony, G.; Fauvage, B.; Falcon, D.; Canet, C.; Dilou, H.; Lavagne, P.; Jacquot, C.; Payen, J. *Crit. Care Med.* **2008**, *36*, 795−800.

(38) Currie, M.; Leopold, H.; Schwarz, J.; Boersma, A. J.; Sheets, E. D.; Heikal, A. A. *J. Phys. Chem. B* **2017**, *121*, 5688−5698.

(39) Zhou, H.-X.; Rivas, G.; Minton, A. P. *Annu. Rev. Biophys.* **2008**, *37*, 375−397.

(40) Dhar, A.; Girdhar, K.; Singh, D.; Gelman, H.; Ebbinghaus, S.; Gruebele, M. *Biophys. J.* **2011**, *101*, 421−430.

(41) Gelman, H.; Wirth, A. J.; Gruebele, M. *Biochemistry* **2016**, *55*, 1968−1976.

(42) Girdhar, K.; Scott, G.; Chemla, Y. R.; Gruebele, M. *J. Chem. Phys.* **2011**, *135*, 015102.

(43) Michea, L.; Combs, C.; Andrews, P.; Dmitrieva, N.; Burg, M. B. *Am. J. Physiol. Physiol.* **2002**, *282*, F981−F990.

(44) Munishkina, L. A.; Ahmad, A.; Fink, A. L.; Uversky, V. N. *Biochemistry* **2008**, *47*, 8993−9006.

(45) White, D. A.; Buell, A. K.; Knowles, T. P. J.; Welland, M. E.; Dobson, C. M. *J. Am. Chem. Soc.* **2010**, *132*, 5170−5175.
(46) Guseman, A. J.; Speer, S. L.; Perez Goncalves, G. M.; Pielak, G. J. *Biochemistry* **2018**, *57*, 1681−1684.
(47) Tan, C. S. H.; Go, K. D.; Bisteau, X.; Dai, L.; Yong, C. H.; Prabhu, N.; Ozturk, M. B.; Lim, Y. T.; Sreekumar, L.; Lengqvist, J.; et al. *Science* **2018**, *0346*, 1−11.
(48) Sukenik, S.; Politi, R.; Ziserman, L.; Danino, D.; Friedler, A.; Harries, D. *PLoS One* **2011**, *6*, e15608.
(49) Gao, M.; Estel, K.; Seeliger, J.; Friedrich, R. P.; Dogan, S.; Wanker, E. E.; Winter, R.; Ebbinghaus, S. *Phys. Chem. Chem. Phys.* **2015**, *17*, 8338−8348.
(50) Sukenik, S.; Sapir, L.; Harries, D. *J. Chem. Theory Comput.* **2015**, *11*, 5918−5928.
(51) Goloubinoff, P.; Sassi, A. S.; Fauvet, B.; Barducci, A.; De Los Rios, P. *Nat. Chem. Biol.* **2018**, *14*, 388−395.
(52) Martinez Molina, D.; Nordlund, P. *Annu. Rev. Pharmacol. Toxicol.* **2016**, *56*, 141−161.
(53) Spinelli, J. B.; Yoon, H.; Ringel, A. E.; Jeanfavre, S.; Clish, C. B.; Haigis, M. C. *Science* **2017**, *358*, 941−946.

DOI: 10.1021/jacs.8b04809
J. Am. Chem. Soc. 2018, 140, 10497−10503